

## LEO Spacecraft Charging and Discharging Induced by High Voltage Solar Arrays

Jianguo H<sup>1\*</sup>, Liu Guoqing<sup>2</sup> and Jiang Lixiang<sup>2</sup>

<sup>1</sup>Beijing Institute of Spacecraft Environment Engineering, Beijing 100094, China

<sup>2</sup>Science and Technology on Reliability and Environmental Engineering Laboratory, China

### Abstract

The charging and discharging induced by application of high voltage solar arrays were attracting increasing attentions recently. In this paper the associated models and tests conducted recently are introduced. For the rapid charging observed on International Space Station recently, a model is developed based on Ferguson et al.'s theory and gives satisfactory calculations consistent with the observations. It shows that the rapid charging events are driven by the abrupt increase of the panel voltage at eclipse exit, and also due to the fact that the charging of the cover glasses by the ambient plasma can't response quickly enough to choke off the electron collection of the solar panel, as a result the structure is rapidly charged to a significant potential within a few seconds. The rapid charging is a type of non-equilibrium charging phenomena and will display normal charging when evolving to equilibrium. In the other hand, the discharges induced by high voltage solar arrays generally occur at triple junction in the presence of an inverted potential gradient from the metal to the dielectric. When a primary arc occurs at solar cell string gaps with high string voltage it will induce secondary arc. Both primary and secondary arc thresholds depend on solar array configurations. We tested the dependence through tests and found that application of wide cell gaps and RTV adhesives help to increase the thresholds for both primary and secondary arcs. But for secondary arc, application of RTV adhesives tends to result in more significant permanent sustained arcs although it postpones the arc occurrence.

**Keywords:** High voltage solar arrays; Plasma; Spacecraft charging; Discharging

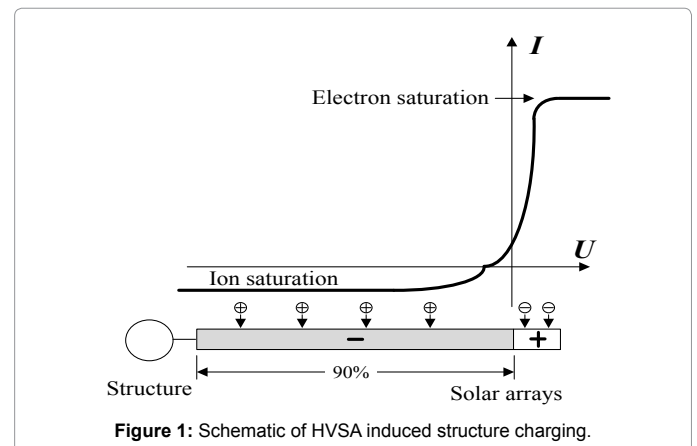
### Introduction

Future space missions will require higher power system. To meet these requirements, either high current or high voltage systems can be used. The use of high current is undesirable for requirement of massive power distribution cables and higher resistive losses during the power transmission. Thus high voltage power generation and transmission at low currents provided by high voltage solar arrays (HVSA) is desirable. However, space crafts with HVSA tend to undergo severe spacecraft charging and discharging issues [1,2]. Especially after the launch of International Space Station (ISS) such issues have attracted increasing concerns.

HVSA induced charging and discharging mainly includes two aspects: Firstly, the interaction of HVSA with space plasma causes the spacecraft to float at a high negative potential, which typically displays as normal charging events (NCEs) or rapid charging events (RCEs). Secondly, HVSA can generate discharges, mainly including primary arc (PA) and secondary arc (SA).

The HVSA induced spacecraft charging had been considered very severe during the early years of ISS operation [3]. Since high voltage solar arrays will collect much more electron currents than ion currents, it was estimated that nearly 90 percent of the solar panels immersed in LEO plasma will float at negative potentials, and the structure electrically connected to the negative end of the panels will consequently float at a significant negative potential as illustrated in Figure 1. This phenomenon is called normal charging events (NCEs). For ISS with 160V HVSA, the normal charging had been estimated to reach nearly -140V. But the FPP [4] (Floating Potential Probe) measured much lower potentials than predicted, generally no more than -25V. The subsequent investigations showed that the charging of the cover glasses by ambient plasma ( $\sim kT_e$ ) and the formed potential

barrier choked off the electron collection by the solar panels, resulting in much lower floating potentials than predictions [5,6]. However, with the assembly of FPMU (Floating Potential Measurement Unit) on ISS in 2006, which has higher resolution than FPP a more severe charging phenomenon was observed, which occurred at exit from eclipse with floating potential rapidly rising to a significant level within a few



\*Corresponding author: Jianguo H, Beijing Institute of Spacecraft Environment Engineering, Beijing 100094, China, E-mail: [huangjg2012@163.com](mailto:huangjg2012@163.com)

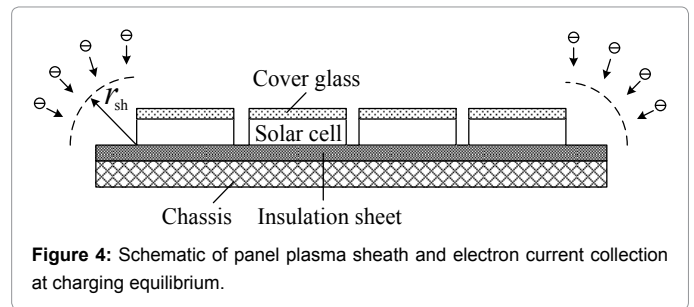
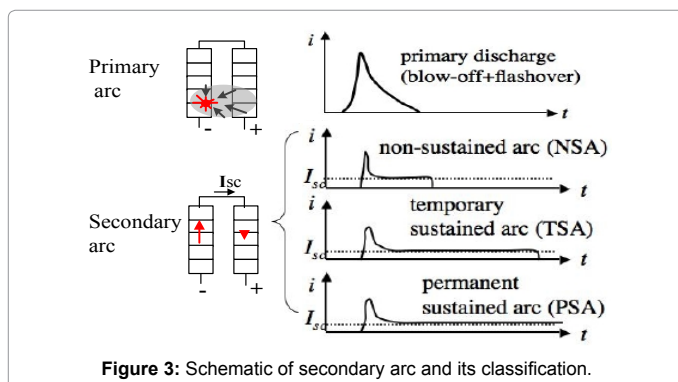
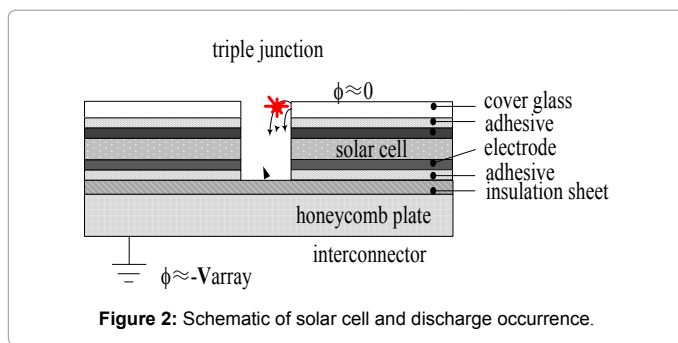
Received January 20, 2015; Accepted March 02, 2015; Published March 30, 2015

Citation: Jianguo H, Guoqing L, Lixiang J (2015) LEO Spacecraft Charging and Discharging Induced by High Voltage Solar Arrays. J Astrophys Aerospace Technol 3: 111. doi:10.4172/2329-6542.1000111

Copyright: © 2015 Jianguo H, et al. This is an open-access article distributed under the terms of the Creative Commons Attribution License, which permits unrestricted use, distribution, and reproduction in any medium, provided the original author and source are credited.

seconds (maximum of -70V observed till now) [7]. This phenomenon is called rapid charging events (RCEs). Most of the RCEs were well above the safety level -40V. The RCEs haven't been thoroughly understood till now. Ferguson et al. have presented a primary theory [8], which thinks that the rapid events are non-equilibrium charging phenomena driven by the abrupt turn on of the solar panels when suddenly entering the sunshine at eclipse exit, and they also provided approximate methods for current collections in the theory. Based on Ferguson et al.'s theory we have developed a physical model quantitatively predicting the charging pulse and its characteristics, with results in good agreement with observations [9,10].

Apart from charging, HVSA also induces specific discharging, which takes place at the metal-dielectric-plasma interface (triple junction) in the presence of an inverted potential gradient (IPG) from the metal to the dielectric. The discharge is generally classified as primary arc (PA) and secondary arc (SA). When the structure floats at a significant negative potential while the cover glasses float at nearly zero (charged to  $-kTe \approx 0$  by LEO plasma) an inverted potential gradient is set up between the interconnectors and cover glasses, which constructs a strong electric field in the narrow gaps and induces enhanced field electron emission (EFEE) [11,12] from the metals. The emitted electrons bombard the sides of cover glasses and cause them to be charged positively due to their high secondary electron emission (SEE) rates, which further enhances the local electric field until an arc takes place. This phenomenon is called primary arc (PA), which is illustrated in Figure 2. If PA occurs between solar cell strings of high voltage difference, a secondary arc (SA) may happen as shown in Figure 3 (left plot). SA is further classified as non-sustained arc (NSA), temporary sustained arc (TSA) and permanent sustained arc (PSA) (right-hand side plot). The secondary arcs will result in power loss and the permanent arcs can lead to significant power degradation, even failure of mission [13,14]. Statistics showed that nearly 33 percent of the mission failures can be attributed to abnormal due to HVSA [15].



Hastings and Cho et al. have successively developed theories for the discharge evaluation [2,11,12].

In this paper we will introduce our theoretical and experimental investigations for the HVSA induced charging and discharging.

### HVSA Induced Spacecraft Charging

Many types of charging events have been observed on ISS, some of which are not related to HVSA, for example, the geomagnetic induction  $\varphi = v \times B \cdot I$  and aural charging. The charging specific to HVSA includes normal charging and rapid charging at eclipse exit.

#### Normal charging

Normal charging is a phenomenon that is driven by HVSA after eclipse exit to a state of charging equilibrium, and is determined by the balance equation:

$$I_e - I_i = I_e - (I_{i-Arr} + I_{i-Str}) = 0, \quad (1)$$

$I_e$  is the electron current collected by the positively biased parts of the panels.  $I_i$  is the ion current and it contains two parts:  $I_{i-Arr}$ , the current collected by the positive parts of the panels, and  $I_{i-Str}$ , collected by the structure. In the following we will discuss the current calculations for ISS condition.

#### A) Electron current $I_e$

$I_e$  is collected by the exposed conductors on the solar panels mainly including interconnectors and sides of solar cells. When the cover glasses are charged to equilibrium by ambient plasma, the electrons to the conductors between neighboring solar cells are blocked by the potential barriers above the cover glasses, and only the outermost sides can collect electrons from space through the sheath around them. The sheath can be approximately treated as quarter cylindrical surface, as illustrated in Figure 4, then we obtain:

$$I_e = A_{SA} \int_0^{160-|\phi|} \pi r_{sh} J_{e0} \frac{dV}{160}, \quad (2)$$

Where  $J_{e0}$  is thermal electron current density:  $J_{e0} = N_e e (kT_e / 2\pi m_e)^{1/2}$ .  $r_{sh}$  is the sheath radius.  $V$  is voltage distribution along the panels.  $\phi$  is the structure floating potential.  $\int_0^{160-|\phi|} \frac{dV}{160}$  represents the integral from the voltage terminator ( $V=0$ ) to the positive end ( $160V-|\phi|$ ) along the panels.  $A_{SA}$  is the exposed conducting area of the panels. According to the orbit-limited theory [16], the sheath radius is:

$$r_{sh} = \left( \frac{eV}{kT_e} \right)^{1/2} \lambda_d, \quad (3)$$

here,  $\lambda_d$  is Derby radius. The sheath has variable radius along the panels length.

### B) Ion current $I_{i-Arr}$ and $I_{i-Str}$

For LEO spacecraft, ion thermal velocity is far smaller than that of the vehicle, hence the negatively biased parts of the panels collect ram ions with vehicle velocity  $v_s$ :

$$I_{i-Arr} = A_{SA} \int_0^\phi J_{i0} \frac{dV}{160}, \quad (4)$$

here,  $J_{i0} = N_e e v_s$  is ram ion current density.

To calculate the ion current by structure  $I_{i-Str}$ , it's necessary to take into account the shapes of the exposed conductors on the structure. For ISS, these conductors mainly include tensioning wires on solar panel masts and they are approximately treated as cylindrical rods. For biased cylindrical conductor the ion current density is focused:

$$I_{i-Str} = A_{Str} \cdot \frac{1}{2} J_{i0} \left(1 + \frac{\phi}{T_i^*}\right)^{1/2}, \quad (5)$$

where,  $A_{Str}$  is the exposed conducting area on the structure. The factor 1/2 is due to the fact that only half the cylindrical surface is collecting ram ions.  $T_i^*$  is an equivalent temperature for ram ion energy  $m_i v_s^2/2$ .

The configuration parameters are important for calculations, and the related variables taken from ref. [8]:  $A_{SA}=7.5m^2$ ,  $A_{Str}=6.3m^2$  and  $T^*=4.89eV$ .

### C) Result

Substitute formula (2), (3) and (4) into Eq.1, the floating potential is obtained. The result for normal charging potential as a function of plasma density is presented in Figure 5, the values agree well with ISS observations [3,7]. The calculation only focus on the approximate charging level, without taking into account some details like spacecraft attitude, etc.

### Rapid charging

Rapid charging occurs within a few seconds (typically 1~3s) at exit from eclipse and is driven by the abrupt switch-on of solar panels in sunshine. It is a non-equilibrium charging state and doesn't satisfy the current balance equation. The rapid charging can be described by the following equation [9,10]:

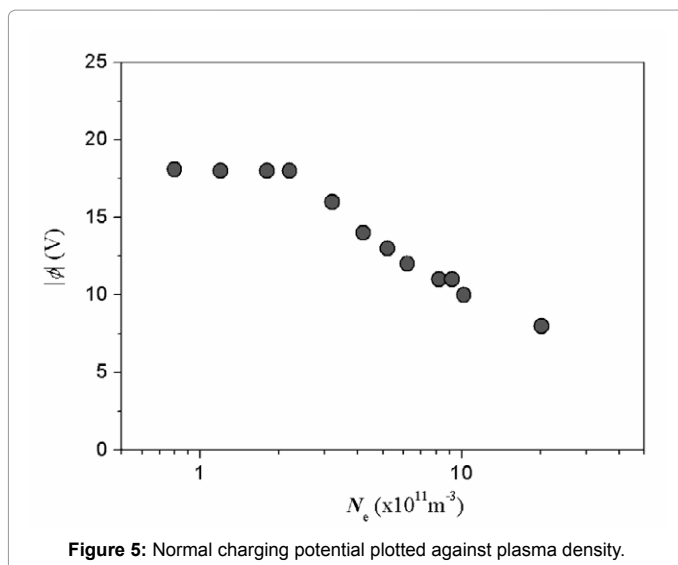


Figure 5: Normal charging potential plotted against plasma density.

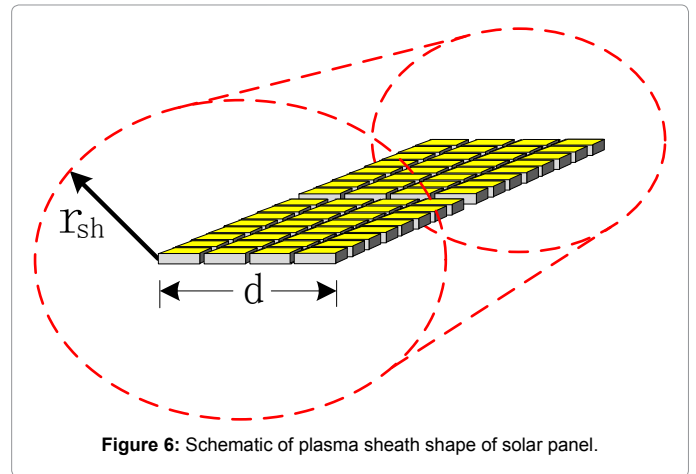


Figure 6: Schematic of plasma sheath shape of solar panel.

$$A_{SA} \int_0^{V_0-\phi} J_{e-SA} \frac{dV}{160} - A_{SA} \int_0^\phi J_{i-SA} \frac{dV}{160} - A_{Str} J_{i-Str} = C_s \frac{d\phi}{dt}, \quad (6)$$

The first item in the left side is the electron current collected by the positively biased parts of the solar panels, and  $J_{e-SA}$  is the electron current density. The second item is the ion current by the negative part of the panels, and  $J_{i-SA}$  is the associated ion current density. The third item is the current by the structure, and  $J_{i-Str}$  is the associated current density.  $V_0$  is the panel voltage, which is distributed linearly along the panel length.  $C_s$  is the structure capacity with respect to space plasma.

### A) Electron current density $J_{e-SA}$

The RCEs generally occurred in a LEO plasma density of  $\sim 10^{10} m^{-3}$ . The panel plasma sheath dimension according to formula (3) is much larger than the panel width  $d$  (for ISS,  $d=0.32m$ ), hence the sheath can be treated approximately as circular cylindrical surface with varying radius along the panel length, as illustrated in Figure 6. The electron current entering the sheath is supposed to be uniformly distributed to the exposed conductors along the width of the panels. The blocking effect on the current to the cell stitches is described by an exponentially attenuating factor  $\sim \exp(-t/\tau_{ch})$ , in which  $\tau_{ch}$  is the blocking timescale. For ISS, the panels constitute four columns of solar cells as illustrated in Figure 6, and the blocked conductors take up approximately 7/8 of the exposed conducting area, hence

$$J_{e-SA}(V) = \frac{\pi r_{sh}}{d} \left[ \frac{1}{8} J_{e0} + \frac{7}{8} J_{e0} \exp(-t/\tau_{ch}) \right], \quad (7)$$

### B) Ion current density $J_{i-SA}$ and $J_{i-Str}$

Similar to the analysis in 2.1, the ion current density collected by the negatively biased parts of the solar panels is (planar model):

$$J_{i-SA} = J_{i0} = N_e e v_s, \quad (8)$$

For the exposed conductors (wires) on ISS structure, the ion current density is (cylindrical model):

$$J_{i-Str}(\phi) = \frac{1}{2} J_{i0} \left(1 + \frac{\phi}{T_i^*}\right)^{1/2}, \quad (9)$$

### C) Panel voltage driving effect

The rapid charging is driven by the sudden switch-on of the panel voltage  $V_0$  in sunshine at eclipse exit.  $V_0$  can be expressed as a function rising up linearly to saturation in a period  $t_0$ :

$$V_0(t) = \begin{cases} V_{0\max} \frac{t}{t_0}, & t \leq t_0 \\ V_{0\max}, & t \geq t_0 \end{cases}, \quad (10)$$

Another reasonable switch-on pattern is exponential ramp up:

$$V_0(t) = V_{0\max} (1 - e^{-t/t_0}), \quad (11)$$

here,  $V_{0\max}$  is the saturated panel voltage, and for ISS,  $V_{0\max} = 160V$ .

#### D) Result

Two typical results with different solar panel switch-on patterns are presented in Figures 7 and 8, with the plasma condition  $N_e = 2 \times 10^{10} m^{-3}$ ,  $T_e = 0.173 eV$ . The pulses agree very well with ISS observations [8-10]. In Figure 9 the further floating potential against plasma density is provided, which is also consistent with the ISS data [8].

Rapid charging is mainly caused by two aspects: first, the solar panel is suddenly switched on in sunshine at exit from eclipse and the panel voltage ramps up rapidly, which generates a rapid electron current collection and subsequent floating potential rapid increasing. On the other hand, the charging of the cover glasses by the ambient plasma can't follow the sudden rise of the panel voltage to block the electron current collection in time. The above two effects add up to result in a significant potential rise within a few seconds. It can be seen from the

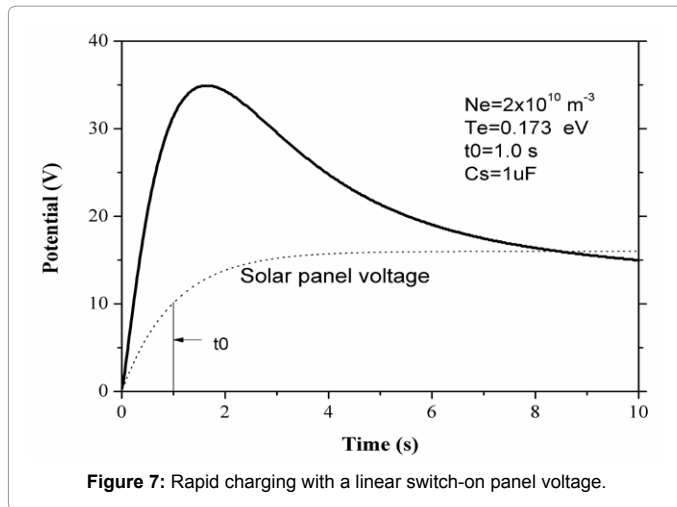


Figure 7: Rapid charging with a linear switch-on panel voltage.

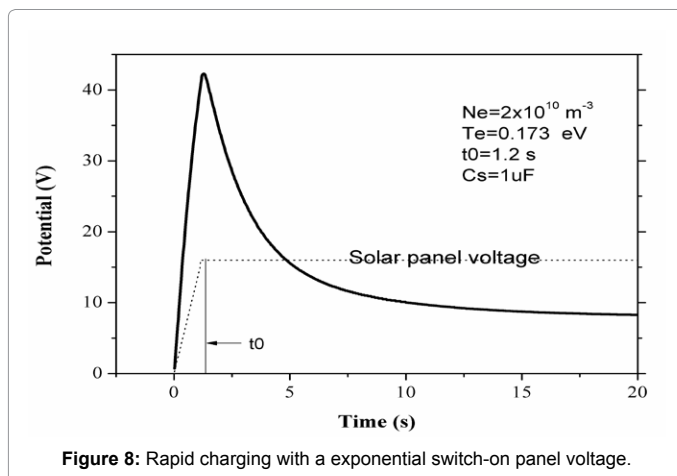


Figure 8: Rapid charging with an exponential switch-on panel voltage.

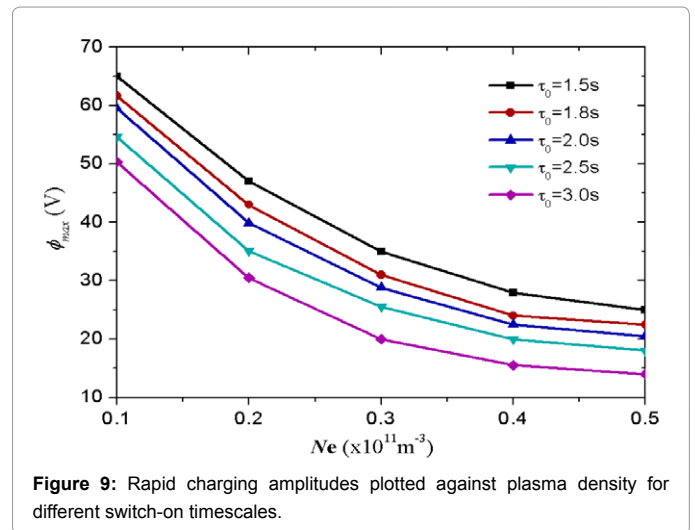


Figure 9: Rapid charging amplitudes plotted against plasma density for different switch-on timescales.

plots that as the rapid event evolves to equilibrium it will display as a normal charging event.

## HVSA Induced Discharging

### Physical model and mechanism

For HVSA induced discharge, Hastings D. E. and Cho M. have developed semi analytical model [2,17]. According to the model, the physics for primary arc (PA) can be described as follows:

A) Primary arc occurs in the vicinity of the dielectric-conductor-plasma interface (triple junction). When ambient ions charge the dielectric front surface to equilibrium a strong electric field of  $E \approx |V_0|/d$  is created at the triple junction where  $V_0$  is the bias potential on the conductor and  $d$  is the thickness of the dielectric.

B) If there is an emission site with high field enhancement factor on the conductor surface near the triple junction, then electrons can be emitted profusely and can charge the side surface. This charging due to enhancement field electron emission (EFEE) charges the side of the dielectric positive and can therefore enhance the electric field at the triple junction further. It can develop very rapidly because of the strong exponential dependence of the current on the electric field.

C) When the electric field doubles, the emission current increases by orders of magnitude. This incident electrons can desorb a significant amount of neutral gas from the surface and dense neutral cloud as high as  $10^{23} m^{-3}$  over the surface. The electrons flowing through the neutral cloud can lead to an avalanche discharge. Even if there is not a dense neutral cloud created over the dielectric, the electric field just over the surface may still increase to the point where dielectric breakdown occurs or a thin layer along the side of the dielectric.

Once the charging time of the dielectric cover glass is known, the arcing rate for a given solar array can be calculated. The inverse of the time which is necessary to build up the electric field is defined as the arcing rate. A schematic picture of the system is shown in Figure 10. According to the above physics, the rate for the electric field at the emission site  $E_e$  can be obtained:

$$\frac{dE_e}{dt} \sim \frac{\sqrt{S}}{C_{diel} d_i^2} (\gamma_{ee} - 1) j_{ec}, \quad (12)$$

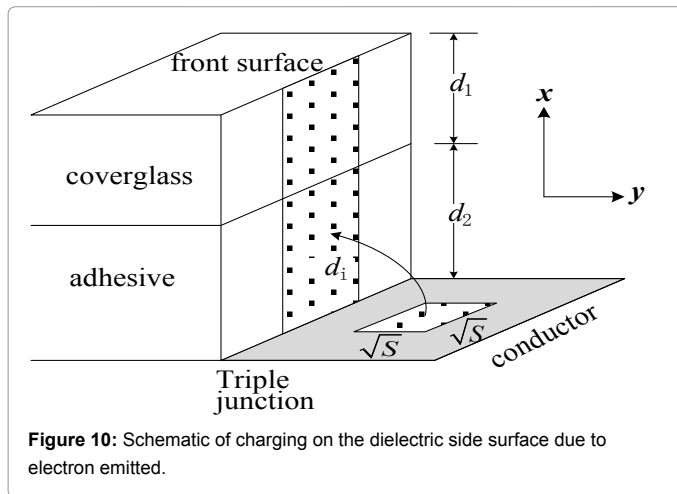


Figure 10: Schematic of charging on the dielectric side surface due to electron emitted.

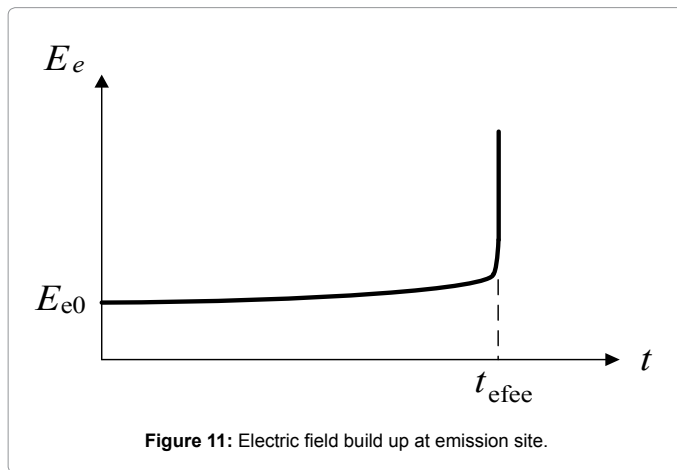


Figure 11: Electric field build up at emission site.

Where  $\gamma_{ec}$  is secondary electron coefficient for cover glass,  $j_{ec}$  is the emission current density.  $C_{diel}$  is the capacitance of the side surface of the dielectric,  $S$  is the emission site area, and  $d_i$  is the impact point on the side surface.  $j_{ec}$  is determined according to EFEE physics:

$$j_{ec} = A'(\beta^2 E_e^2) \exp\left(-\frac{B}{\beta E_e}\right), \quad (13)$$

where  $\beta$  is EFEE ratio, and other parameters are constants.

The field on the emission site builds up as in Figure 11, an arc takes place at the moment of  $t=t_{efee}$ . The arcing rate is calculated:

$$\gamma = \frac{1}{t_{efee}}, \quad (14)$$

### Primary arc

The rate for primary arc (PA) strongly depends on the solar panel configuration, so needs to be evaluated according to specific application and missions. The test circuit for PA is shown in Figure 12. The primary discharge is mainly determined by the biased voltage, cell gap and other macroscopic parameters, but weakly dependent on string voltage. Therefore, to simplify the arc test without affecting the result, the four strings are connected in parallel.  $C_{ext}$ ,  $R_{ext}$  and  $L_{ext}$  are used to generate arc pulse with necessary shape. Considering a  $2m \times 5m$

solar paddle and assuming a peak current of 1.5 pA and duration of 500  $\mu s$  for the worst case,  $C_{ext}$ ,  $R_{ext}$  and  $L_{ext}$  are calculated to be 2  $\mu F$ , 94 $\Omega$  and 8 mH, respectively. The limitation resistance  $R_b$  is taken 10k $\Omega$ . Current probe CP1 is used to monitor the discharge between solar cells and face sheet, and CP2 to CP3 to monitor arcs occurring in cell gaps. Any of the arcing events can be caught by CP4. The test was conducted in a  $\phi 1.3m \times 13m$  LEO plasma simulator with the plasma environment  $N_e \sim 10^5 - 10^9 \text{ cm}^{-3}$ ,  $T_e < 5eV$ .

To investigate the dependence of threshold voltage for primary arc on solar panel configurations, we manufactured four coupons different in cover glass thickness, string gap and RTV application as displayed in Table 1. The result shows that each configuration parameter has different significance to threshold voltage. In order to differentiate the significance, we define a weighting factor  $\alpha_A$  for each parameter:

$$\alpha_A = 1 + (\Delta V / V_0) / (\Delta A / A_0), \quad (15)$$

Here  $A$  is the configuration parameter, e.g. cover glass thickness, string gap, RTV application or not. For application of RTV,  $A=1$ , otherwise  $A=0$ .  $V$  is the threshold voltage.  $\Delta V / V_0$  and  $\Delta A / A_0$  are relative variations normalized by the parameter of coupon 1#, which is a standard coupon. The weighting factors for string gap, RTV application and cover glass thickness are calculated to be 1.19, 1.25 and 1.49, respectively. Then  $\alpha_A$  can be used to rank the four coupons in order of significance. The variation of threshold voltage for different configurations is illustrated in Figure 13, the result shows that in

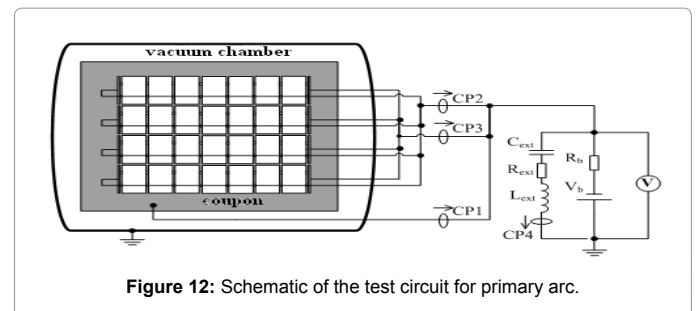


Figure 12: Schematic of the test circuit for primary arc.

No.	Glass Thickness	String Gap	RTV on Interconnector	Threshold Voltage	$\alpha_A$
1	0.12 mm	0.9 mm	NO	-80V	1.00
2	0.30 mm	0.9 mm	NO	-90V	1.19
3	0.12 mm	1.5 mm	NO	-110V	1.56
4	0.12 mm	0.9 mm	Yes	-100V	1.25

Table 1: PA thresholds for different solar panel configurations.

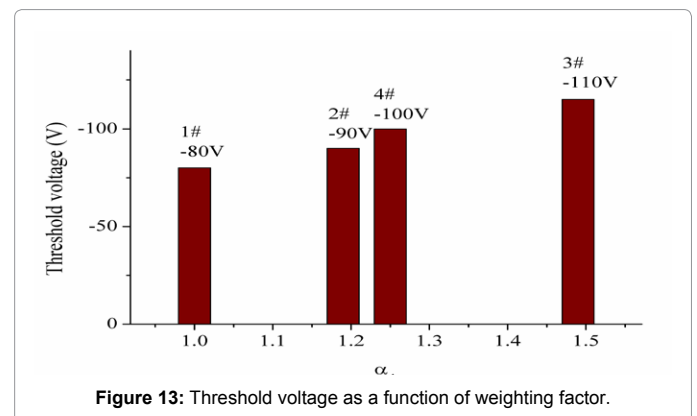


Figure 13: Threshold voltage as a function of weighting factor.

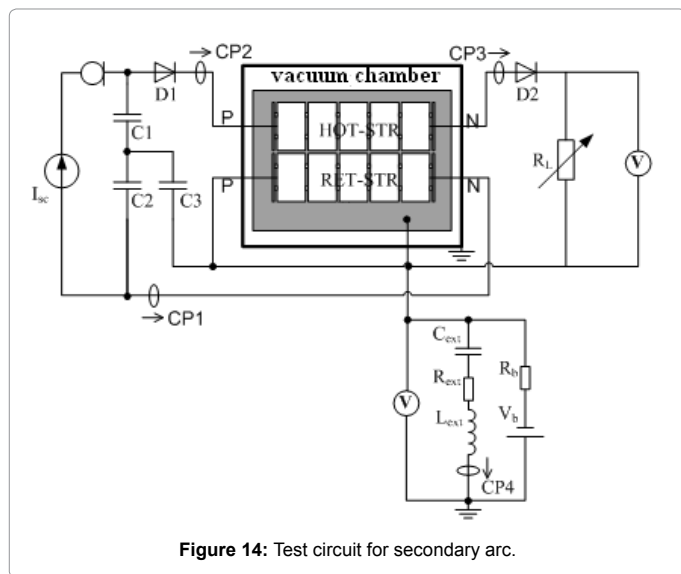


Figure 14: Test circuit for secondary arc.

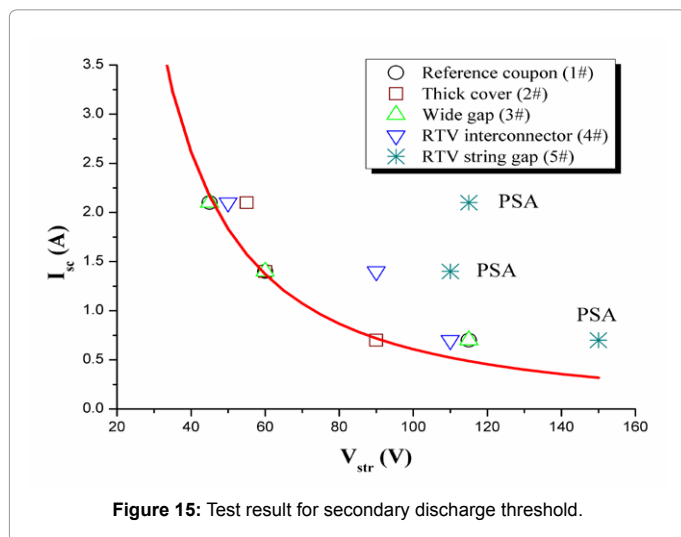


Figure 15: Test result for secondary discharge threshold.

ameliorating primary arc, most effective is application of wide cell gap, then RTV adhesive and last thick cover glass.

### Secondary arc

Secondary arc is induced by primary arc at high enough string voltage. The circuit for secondary arc test is shown in Figure 14. The current source is used to simulate the power generated by the solar paddle. The insertion of a diode is to protect the power supply from the primary discharge.  $C_1$ ,  $C_2$  and  $C_3$  are used to simulate face sheet capacitance and string capacitance, respectively. The face sheet capacitance is the capacitance between the solar cells and the conductive substrate through the adhesive and insulation sheet. The string capacitance is the capacitance associated with the differential mode between the two ends of the string. Both the capacitances are calculated from the number of cells and strings of a solar array paddle, with their values  $C_1 = C_2 = 20\text{nF}$  and  $C_3 = 21\text{nF}$ .  $R_L$  corresponds to a load of satellite. Probe CP1 to CP3 are to detect arc currents flowing through the string loop and CP4 is to probe the PA current pulse.

The threshold test result of secondary is shown in Figure 15. Five coupons were tested all together. Apart from the four samples in

Table 1, another coupon with RTV adhesive between string gaps (5#) was tested. In Figure 15, the red curve denotes the threshold of secondary arc, which is a combined condition of  $V_{str}$  and  $I_{sc}$ . All the SA data fall above the threshold line. The fitting function of the threshold curve is  $y = ax^b$  with  $a = 921.5$  and  $b = -1.6$ . Compared with the standard coupon (1#), thick cover glass (2#) and wide string gap (3#) have little influences on SA threshold although they have apparent effects to PA (Figure 13). The remarkable phenomenon is that application of RTV adhesive increases the threshold significantly (4# and 5#). It's also notable that although RTV application postpones the secondary arc to higher threshold, the induced secondary arc, once coming forth, tends to display as permanent sustained arc (PSA).

### Summary

HVSA induced charging and discharging is specific issues due to application of high voltage array. In the paper the major theories, mechanisms and tests are introduced.

HVSA can induce charging of structure due to its interaction with LEO plasma. The normal charging events have much lower levels than expected before because the charging of cover glasses blocks the electron current collection by the solar panel. However the rapid charging which occurs at exit of eclipse can reach high level due to the fact that the blocking effect can't follow the rapid rise of the panel voltage that is switched on suddenly in sunshine. The model for RCEs gives predictions in good agreement with ISS observations.

The HVSA induced discharge takes place specifically at metal-dielectric-plasma interface (or triple junctions), where the presence of inverted potential gradient induces electron emission due to EEEE effect. The emission electrons impart on the side dielectric with high SEE ratio and a strong electric field builds up so as to result in primary arc. If primary arc occurs between neighboring strings with high voltage difference, secondary arc may occur. Both PA and SA occurrence depend on solar panel configuration. Test results show that application of wide cell gap, RTV adhesive can increase thresholds for PA and SA. But for SA, although application of RTV adhesive postpones SA to higher threshold, it also bring more significant arc once the arc happens.

### References

1. Tribble AC, Low Earth Orbit Plasma Effect on Spacecraft, AIAA93-0614.
2. Hastings DE, ChoM, The Arcing Rate for a High Voltage Solar Array: Theory, Experiment and Predictions. AIAA92-0576.
3. Carruth MR, Schneider T, JrMcCollum M, Finckenor M, Suggs R (2001) ISS and Space Environment Interactions Without Operating Plasma Contactor, AIAA-2001-0401, 39<sup>th</sup> AIAA Aerospace Sciences Meeting & Exhibit, 8-11 January 2001/Reno, NV.
4. Ferguson DC, Morton TL, Hillard GB (2001) First Results from the Floating Potential Probe (FPP) on the International Space Station, AIAA 2001 -0402, 39<sup>th</sup> Aerospace Sciences Meeting & Exhibit January 8-11, 2001 / Reno, NV.
5. Kennerud KL, HighVoltage Solar Array Experiments. NASA-CE-121280, High Voltage Final report.
6. Guidice DA, Davis VA, Cutis HB, Ferguson DC, Hastings DE, et al. (1997) Photovoltaic Array Space Power Plus Diagnostics (PASO Plus) Experiment. PL-TR-97-1013, Final Report.
7. Minow JI (2010) Summary of 2006 to 2010 FPMU Measurements of International Space Station Frame Potential Variations. 11<sup>th</sup> Spacecraft Charging Technology Conference Albuquerque, New Mexico.
8. Ferguson DC, Craven P, Minow JI (2009) A Theory for Rapid Charging Events on the International Space Station. 1<sup>st</sup> AIAA Atmospheric and Space Environments Conference, San Antonio, TX.

9. Huang Jianguo, Yi Zhong, Zhao Hua, Meng Lifei, Liu Yenan (2014) A Model of Rapid Charging Events for International Space Station *Journal of Spacecraft and Rockets* 51: 11-15.
10. Huang Jianguo, Yi Zhong, Zhao Hua, Meng Lifei, Liu Yenan (2014) Mechanism of Rapid Charging Events for ISS. *Journal of Spacecraft and Rockets* 51: 917-921.
11. Chao M (1992) Arcing on High Voltage Solar Arrays in Low Earth Orbit: Theory and Computer Particle Simulation *53*: 1883.
12. Hastings DE, Weyl G, Kaufman D (1992) The Threshold Voltage for Arcing on Negatively Biased Solar Arrays. *Journal of Spacecraft and Rockets* 27: 538-554.
13. Grier NT, John Stevens N (1987) Plasma Interaction Experiment (PIX) Flight Results. *Spacecraft Charging Technology. NASA CP-2071*: 295-314.
14. Grier NT (1983) Plasma Interaction Experiment II: Laboratory and Flight Results. *Spacecraft Environment Interactions Technology Conference*: 333-348.
15. Frost, Sullivan (2004) Commercial Communications Satellite Bus Reliability Analysis.
16. Rodgers D (2004) *Spacecraft Plasma Interaction Guidelines and Handbook. European Space Agency* 30: 19.
17. Cho M, Hastings DE (1991) Dielectric Charging Processes and Arcing Rates of High Voltage Solar Arrays. *Journal of Spacecraft and Rockets* :698-709.